Computers and Geotechnics 71 (2016) 283–294

Contents lists available at ScienceDirect

Computers and Geotechnics

journal homepage: www.elsevier.com/locate/compgeo

Application of distinct element methods to simulation of hydraulic fracturing in naturally fractured reservoirs

Branko Damjanac *, Peter Cundall

Itasca Consulting Group, Inc., 111 Third Avenue South, Suite 450, Minneapolis, MN, United States

ARTICLE INFO

Article history:
Available online 29 July 2015

Keywords:
Numerical
Modeling
Hydraulic
Fracturing

ABSTRACT

The Distinct Element Method (DEM) represents a rock mass as an assembly of blocks (polygonal or polyhedral). Contacts between blocks correspond to discontinuities (i.e., fractures or joints) that can exhibit non-linear mechanical behavior, including slip and opening. If flow in rock fracture is approximated using the lubrication equation, coupled hydro-mechanical DEM models can be used for simulation of rock mass treatment by fluid injection. However, this approach has a limited capability for simulating fracture propagation. The synthetic rock mass (SRM) concept overcomes this limitation. In SRM, the bonded particle model (BPM), which is an assembly of circular or spherical particles bonded to each other, represents deformation and damage of intact rock. If pre-existing discontinuities are represented in the BPM, the resulting model, referred to as SRM, has the capability of simulating hydraulic fracturing in naturally fractured reservoirs. The model delivers a pattern of hydraulic fractures that evolves in response to both intact rock fracturing and sliding and opening of pre-existing joints.

1. Introduction

Extraction of the abundant reserves of shale gas and oil around the world has been made economical over the last 15 years because of advances in two technologies: horizontal drilling and multi-stage hydraulic fracturing [1]. Multi-stage fracturing from a horizontal section of a wellbore, commonly 700–3000 m in length, allows effective stimulation of the production horizon. Although hydraulic fracturing has been used in successful commercial applications in conventional reservoirs since 1949, there is still a lack of understanding of the hydraulic fracturing effects in these very low permeability, "unconventional" reservoirs. This often leads to unreliable well completion designs.

The main difficulties in achieving reliable completion design arise from: (1) complexity of the physical processes involved, (2) geological complexity, uncertainty and spatial variability, and (3) relatively limited access (typically a single wellbore) to the treated formation. Even hydraulic fracturing of a formation that can be idealized as homogeneous, isotropic, and continuous involves complex, non-linear, hydro-mechanical processes occurring on different length scales. Shale gas and oil reservoirs, on the length and time scales of interest during hydraulic fracturing stimulations, cannot be approximated properly as homogeneous or continuous. Hydraulic fracturing and stimulation of shale formations are critically affected by the interaction between the hydraulic fracture and the discrete fracture network (DFN). This interaction affects not only the speed of hydraulic fracture propagation, but also the stimulation of the reservoir characterized by the extent to which the DFN undergoes inelastic deformation (i.e., slip and opening). Thus, in order to be able to analyze and design a hydraulic fracturing treatment, it is necessary to have analytical tools capable of simulating propagation of fluid-driven fractures in discontinuous (already fractured) rock masses.

Limited access to the simulated formation is an additional challenge to modeling hydraulic fracturing. There is considerable uncertainty in the characterization of the rock mass and particularly of the DFN. Also, due to relative inaccessibility, interpretation of the model results and model calibration to the response of a particular reservoir is difficult and uncertain. The injection pressure and microseismic data are usually the only information available to assess the response of deep reservoirs to fluid injection. Thus, it is essential that the numerical models (besides capabilities to explicitly represent a DFN and to predict injection pressures) can also generate synthetic microseismicity. Such models can be used as components of fracture network engineering (FNE), discussed briefly in Section 2. FNE is a methodology that promises to provide a robust approach for designing fractured rock mass stimulation by fluid injection.

* Corresponding author.
E-mail addresses: branko@itascacg.com (B. Damjanac), pacundall@aol.com (P. Cundall).

http://dx.doi.org/10.1016/j.compgeo.2015.06.007
0266-352X/

For years, the distinct element method (DEM), originally developed by Cundall [2], has been used in different industries (e.g., mining, civil and nuclear waste disposal) to solve problems involving stability of fractured rock masses. Some of the initial applications of DEM to problems of hydraulic treatment of the rock mass were conducted by Pine and Cundall [3]. These models were fully coupled hydro-mechanically and flow in rock joints was approximated by the lubrication equation [4]. They were best suited for problems of fluid flow through a DFN coupled with deformation of fractured rock mass. Typically it was assumed that pre-existing fractures did not propagate.

3DEC [5] is a three-dimensional (3D) distinct element code for simulation of a general mechanical interaction of polyhedral solid blocks. The blocks can be assumed to be rigid or fully deformable. An assembly of tightly packed blocks approximates fractured rock mass with the contacts between blocks representing the rock joints. The contacts can deform elastically or inelastically, resulting in opening or slip, typically governed by Coulomb slip law. The formulation of a numerical scheme for resolution of general block interaction and contact detection in 3D was described by Cundall [6]; the formulation of mechanical calculations for motion and interaction between deformable polyhedral blocks as implemented in *3DEC* was described by Hart et al. [7]. A fully coupled 3D numerical model of fluid flow in deformable fractured rock masses was originally implemented in *3DEC* by Damjanac [8]. In recent years, *3DEC* has been used successfully for investigation of the response of fractured rock mass to fluid injection and hydraulic fracturing (e.g., [9]) and prediction of induced microseismicity [10]. These applications demonstrate its suitability as an analytical tool for FNE. An example that illustrates application of the DEM (as implemented in *3DEC*) to simulation of hydraulic fracturing, and the effect and importance of DFN for fracture propagation are presented in Section 3. In the beginning of the same section, *3DEC* results are compared with semi-analytical solution (PKN) in verification of the code and the DEM for simulation of hydraulic fracturing.

Applicability of coupled DEM models to hydraulic fracture propagation is limited to the cases in which the fracture trajectory is known. To overcome the limitation of the original DEM models in which the fracture trajectory needs to be predefined, a new generation tool has been developed. This tool uses the bonded particle model (BPM) [11] and the synthetic rock mass (SRM) concept [12]. It has been developed specifically to model hydraulic fracture propagation in naturally fractured reservoirs. The SRM concept is realized as a bonded-particle assembly containing multiple joints. Each joint consists of a planar array of bonds that obey a special model, namely the smooth joint model (SJM). The SJM allows slip and separation at particle contacts, while respecting the given joint orientation rather than local contact orientations. Overall fracture of a synthetic rock mass depends on both fracture of intact material (bond breaks), as well as yield of joint segments.

Previous SRM models have used the general purpose codes *PFC2D* [13] and *PFC3D* [14], which employ assemblies of circular/-spherical particles bonded together. Much greater efficiency can be realized if a "lattice," consisting of point masses (nodes) connected by springs, replaces the balls and contacts (respectively) of *PFC*. The lattice model still allows fracture through the breakage of springs along with joint slip, using a modified version of the SJM. The new 3D program, *HF Simulator*, described in this paper, is based on such a lattice representation of brittle rock. *HF Simulator* overcomes all of the main limitations of the conventional (including the original DEM) methods for simulation of hydraulic fracturing in jointed rock masses. It is computationally more efficient than *PFC*-based implementations of the SRM method. A description of this novel methodology, its verification, and one example application are presented in Section 4.

2. Fracture Network Engineering (FNE)

In order to understand the rock mass response to fluid injection, we must rely on "indirect" data. These include injection pressure and flow rate as functions of time, microseismic signals (now being monitored and processed more often) and tracer tests during injection/production.

The microseismic data provide information on location, time, magnitude and source mechanisms of local instabilities (events) caused by fluid injection in the rock mass. Although microseismic events may result from either fracturing of the intact rock or seismic slip on pre-existing fractures, the magnitudes of events associated with intact rock fracturing are typically below the threshold of recording equipment, and therefore are not included in the recorded microseismic data [15]. The extent of microseismic activity very often is assumed to correspond to the stimulated rock volume (SRV). Although there should be a correlation, it is not clear that these two volumes are the same [15]. For example, if a microseismic event is caused by change in the total stress, it might not be connected to the wellbore by a continuous high-permeability (i.e., stimulated) region. Microseismic data do not allow a clear distinction to be drawn between events that are caused by total stress change ("dry events") and events caused by fluid pressure change ("wet events").

Proper interpretation of the microseismic signals requires a numerical model that is capable of generating synthetic microseismicity. Such numerical models can be calibrated by comparing the model results with the observed field microseismicity (and the injection-pressure data) until the predicted and observed data are in close agreement. This is the essence of the FNE [16] method. The calibrated model can be used for interpretation of the field microseismicity. Also, forward-looking analysis then can be carried out to simulate how an assumed fracture network will behave for different stimulations with the goal of establishing design criteria for a field project and engineering the most effective fracture network (Fig. 1). Both DEM and the lattice models have the capability of generating synthetic microseismicity, following a similar approach to Hazzard et al. [17].

3. DEM as a component of fracture network engineering

Numerical models based on the DEM can serve as the analytical component in FNE. In the DEM, an assembly of blocks (polygonal or polyhedral) or particles can be used to represent the mechanical behavior of the fractured rock mass. Contacts between the blocks can open or slide to approximate the behavior of pre-existing or newly created fractures. Although the DEM typically does not represent partially fractured blocks or allow fracture propagation through a block, both effects can be achieved by gluing (i.e., assigning certain bond strength in normal and shear directions) some parts of the interfaces between the blocks and allowing progressive failure of the interfaces, as dictated by evolution of the contact stresses during simulation. Detailed formulation of DEM and coupled hydro-mechanical model for simulation of flow in fractured rock mass can be found in *3DEC* technical documentation [5]. A verification test and application example using DEM, as implemented in the *3DEC* numerical code, are presented to demonstrate solution of hydraulic fracturing problems and suitability of the DEM-based models as an analytical tools for FNE.

3.1. Verification test: PKN fracture

In the verification problem, the propagation of a planar vertical hydraulic fracture constrained within a 20-m thick horizontal layer was simulated. Newtonian fluid with 1 cP (10^{-3} Pa s) viscosity was

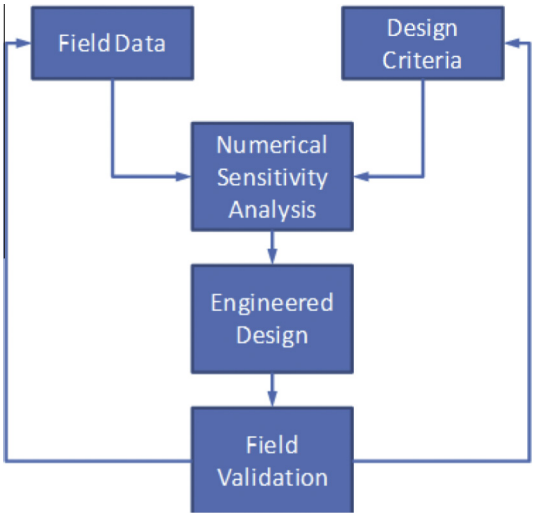

Fig. 1. Fracture Network Engineering (FNE) design cycle.

injected through a vertical wellbore at 2×10^{-3} m^3/s uniformly distributed over the thickness of the layer. The reservoir model is an impermeable, homogeneous, isotropic, elastic medium with Youngs modulus of 10 GPa and Poissons ratio of 0.2.

The evolution of the pressures and fracture widths for this case were approximated using the PKN analytical solution [18]. The geometry of the PKN model and the important model variables are illustrated in Fig. 2.

According to the PKN solution, the net pressure, p_{net}, can be approximated using the following expression:

$$p_{net} = \left[\frac{16\mu q E^3}{(1-\nu^3)^3 \pi H^4}\right]^{1/4} \quad (1)$$

while the expression for the width (aperture) in the middle of the fracture is

$$w(x) = 3\left[\frac{\mu q (1-\nu^2)(L-x)}{E}\right]^{1/4} \quad (2)$$

where E is the Youngs modulus, ν is the Poissons ratio, q is the injection rate, μ is the viscosity of the injected fluid and L and H are the half-length and height of the fracture, respectively, as illustrated in Fig. 2.

The *3DEC* model was constructed using the symmetry of the problem and represented one (upper) half of the fracture only. The trace of the fracture was predefined in *3DEC* by a vertical contact plane, which was joined together initially but allowed to open (fracture) within the constant-height layer during the simulation, as dictated by stress changes induced by the injected fluid. (The vertical contact plane was not allowed to fracture outside the predefined layer.) The fracture plane was the only discontinuity within the model.

The PKN solution is for a fracture in an infinite elastic medium. Because the *3DEC* model size must be finite, the model domain was selected to be sufficiently large compared to the size of the fracture (i.e., fracture height, H, and the fracture half-length, L, achieved during the simulation) such that the deformation of the fracture was not affected by the model size. However, model size effect on the runtime was also considered (because too large of a model would require longer simulation time). The model geometry is illustrated in Fig. 3. "Roller" boundary conditions were applied on all outside boundaries of the mechanical model. The fluid was injected at the specified rate along the vertical edge of the fracture surface as indicated in Fig. 3.

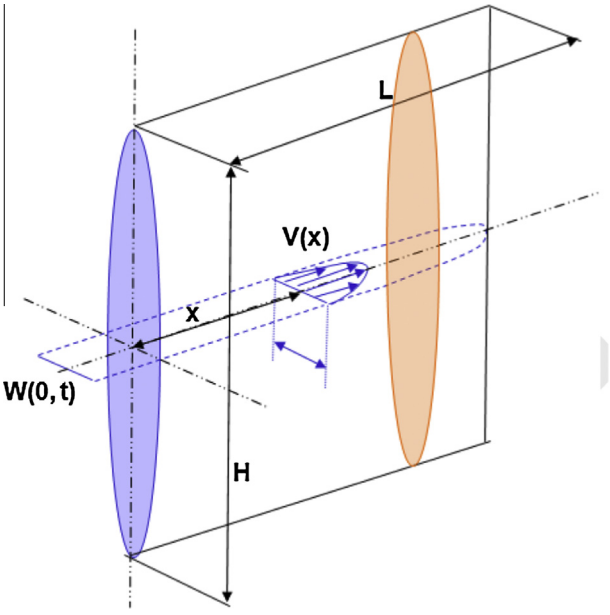

Fig. 2. Geometry of the PKN model.

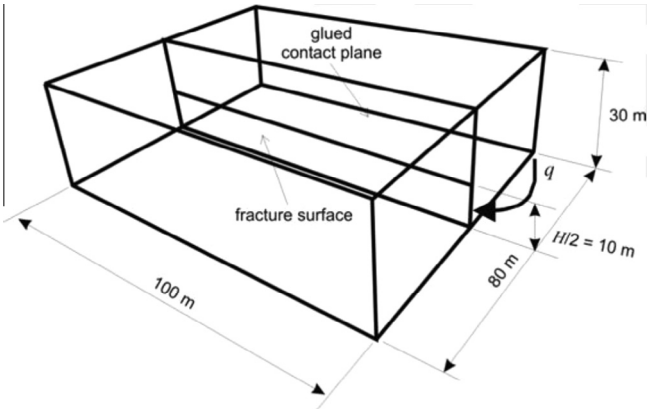

Fig. 3. Geometry of the *3DEC* PKN model.

After the simulation of 368 s of injection, the fracture was approximately 75 m long in the *3DEC* model, which was considered sufficient to satisfy the assumption (i.e., $L/H = 75/20 = 3.75 \gg 1$) used in the derivation of the PKN solution. The state of the *3DEC* model after 368 s of injection, illustrated by the contour fluid pressure and apertures shown in Figs. 4 and 5, respectively, then was compared with the PKN solution. The fluid pressure contours in Fig. 4 illustrate that there was no pressure gradient in the vertical direction, except near the injection point and the fracture tip, as approximated by the PKN solution. The fracture widths (apertures) predicted in *3DEC* and using the PKN solution are compared in Fig. 6.

Overall, the *3DEC* predictions were in reasonably good agreement with the PKN solution. The match of the maximum widths was particularly good near the injection point. As expected, the discrepancy was greatest near the fracture tip. The *3DEC* model consisted of constant-strain zones of uniform size along the entire fracture. Thus, the approximations of the stress singularity and strain gradients near the fracture tip were relatively poor. The second reason for the poor match near the fracture tip was that the minimum fracture aperture in the *3DEC* model cannot be smaller than the user-specified residual aperture. The motivation for this

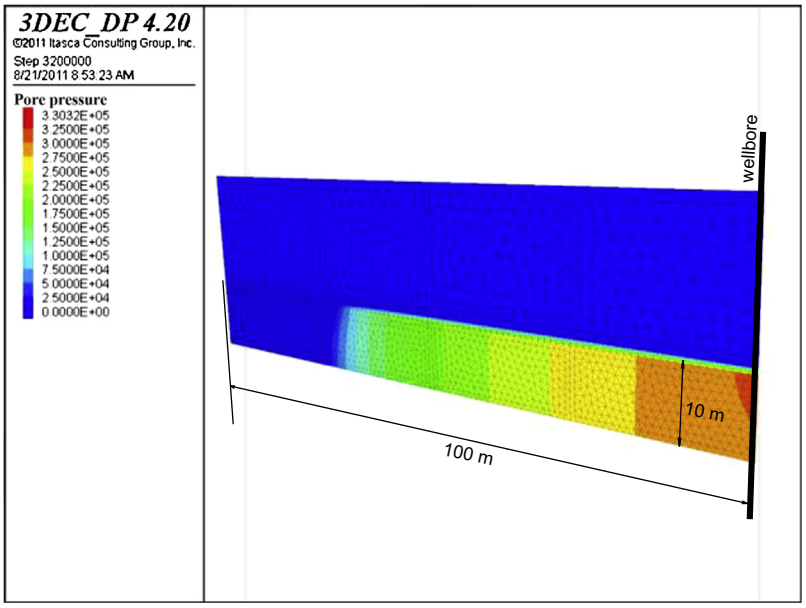

Fig. 4. Fracture pressure contours (Pa) in the fracture plane predicted in the *3DEC* PKN model.

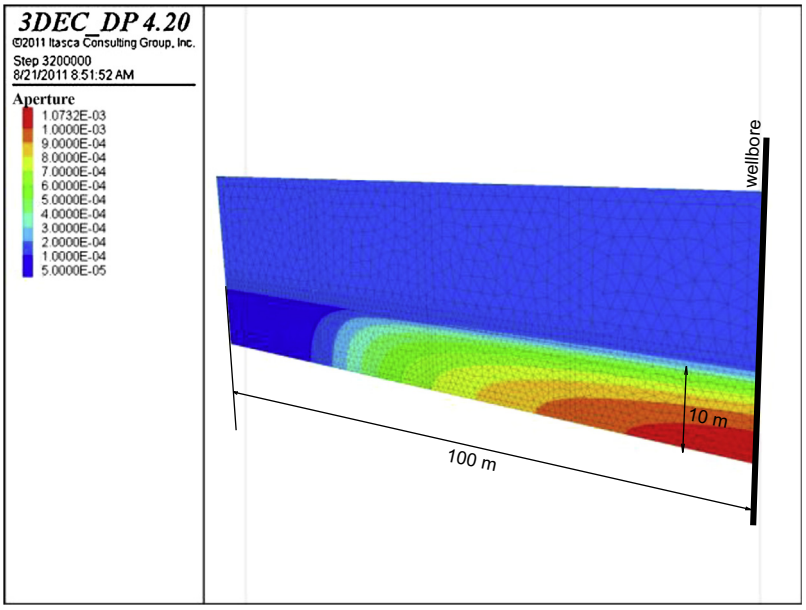

Fig. 5. Fracture width (aperture) contours (m) in the fracture plane predicted in the *3DEC* PKN model.

limit is to prevent model instability when the flow equations become singular as the aperture decreases to zero. Typically, the residual aperture is selected to be small compared to prevailing apertures in the model, and in the simulations the residual aperture was assumed to be 50 μm. Comparisons of the maximum net pressure and fracture widths as calculated using *3DEC* and the PKN solution are provided in Table 1. The match is good, with a maximum error less than 10%.

3.2. Example application

The following example illustrates the application of the 3D DEM code, *3DEC* [5], to a problem of hydraulic fracturing in a naturally fractured reservoir [9]. The goal was to investigate the influence of the DFN connectivity (as a function of fracture size and density) on the way in which the fluid injection affected reservoir stimulation. Two DFNs were used; one fully connected and one sparsely connected, as shown in Fig. 7.

In this example, because of the limitation of DEM that a fracture's trajectory is limited to pre-defined block and contact geometry, the cut is placed in the model through the injection point perpendicular to the minimum principal stress. Initially, the contacts along the surface of the cut were bonded together. During the simulation, those bonds were allowed to break progressively representing propagation of the hydraulic fracture. Thus, although the trajectory of the hydraulic fracture was assumed (perpendicular to the minimum principal stress), the model resolved fracture propagation along that trajectory. Fig. 8 shows a horizontal cross-section (indicated in Fig. 9) through the stimulated reservoir. Distribution of fluid pressure after 50 min of injection is indicated

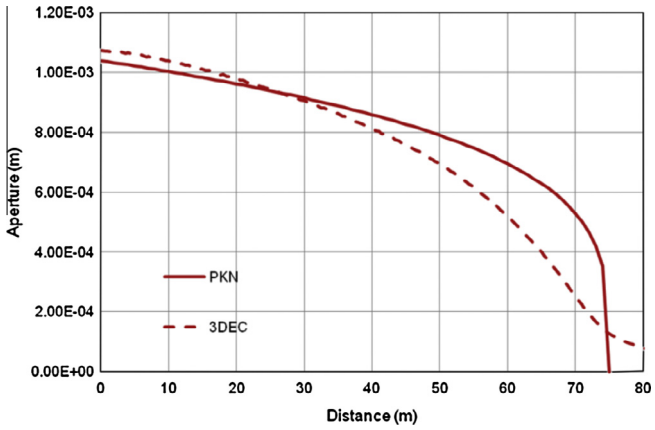

Fig. 6. Profile of the widths (aperture) measured along the fracture half-length at mid-height predicted by the PKN analytical solution and *3DEC*.

by the color scale. The orientations of the horizontal principal stresses are indicated in Fig. 8. Thus, the trace of the hydraulic fracture is through the middle of the model, vertical and perpendicular to the minimum horizontal principal stress ($\sigma_{h\,\min}$).

The plot in Fig. 8 indicates that the better connected DFN results in better stimulation of the naturally fractured reservoir (i.e., the pressures propagate further from the plane of the hydraulic fracture). That result is to be expected. However, the contour plot of the hydraulic fracture apertures (shown in Fig. 9 with pressure contour plot on the surface of the hydraulic fracture limited vertically within the stimulated reservoir) indicates an interesting response. The apertures do not follow the general trend that is expected from classical hydraulic fracture models, such as KGD and PKN [21]. As a result of interaction between the hydraulic fracture and the DFN, and slip on the pre-existing joints intersected by the hydraulic fracture, the apertures in the plane of the hydraulic fracture do not vary smoothly and gradually as usually predicted. Instead, they are very non-uniform and even discontinuous. It is expected that such distribution of apertures will have a significant effect on proppant transport and placement.

4. Synthetic Rock Mass (SRM) approach

4.1. Background

The SRM has been developed [12] as a more realistic representation of mechanical behavior of a fractured rock mass compared to conventional numerical models. The SRM consists of two components: (1) the bonded particle model (BPM) of deformation and fracturing of intact rock, and (2) the smooth joint model (SJM) of mechanical behavior of discontinuities.

The BPM, originally implemented in *PFC*, is created when the contacts between the particles (disks in 2D and spheres in 3D) are assigned certain bond strength (both in tension and shear). It was found that the BPM approximates mechanical behavior of brittle rocks quite well [11]. The elastic properties of the contacts (i.e., contact shear and normal stiffness) can be calibrated to match the desired elastic properties (e.g., Youngs modulus and Poissons ratio) of the assembly of the particles. Similarly, the tensile and shear contact strengths can be adjusted to match the macroscopic strengths under different loading conditions (e.g., direct tension, unconfined, and confined compression).

In the BPM, the contact behavior is perfectly brittle. Breakage of the bond, a function of the forces in the contact and the bond strength, corresponds to formation of a microcrack. An example of an unconfined compression test conducted using *PFC2D* is illustrated in Fig. 10. This figure shows recorded axial stress–strain response and the model configuration with generated microcracks. The shear microcracks are shown in black; the tensile microcracks are shown in red. The state when the sample is loaded beyond its peak strength is shown in the figure. The stress–strain curve exhibits characteristics that are typical of brittle rock response. For loading less than ~80% of the peak strength, the stress–strain response is linearly elastic, with the slope of the line equal to the Youngs modulus. Some microcracks, randomly distributed within the sample, start developing at load levels greater than ~40% of the peak strength. Significant non-linearity develops as the load exceeds 80% of the peak strength. In this phase, the microcracks begin to coalesce, forming fractures on the scale of the sample. After the peak strength is reached, the material starts to soften (i.e., to lose load bearing capacity). At this stage the failure mechanism and the "shear bands" are well developed as shown in Fig. 10. It is well known [19] that in an unconfined compression test, the majority of the cracks are tensile (red[1] lines in Fig. 10). The "shear bands" on the scale of the sample are formed by coalescence of a large number of tensile microcracks.

In order to model a typical rock mass in the BPM, it is also necessary to represent pre-existing joints (discontinuities). A straightforward approach is to simply break or weaken the bonds (in the contacts between the particles) intersected by the pre-existing joints. The created discontinuity will have roughness with the amplitude and wavelength related to the resolution, or the particle size of the BPM. The mechanical behavior of discontinuities is very much affected by their roughness. The problem is that the selected particle size (or resolution) typically is not related to actual roughness of the pre-existing joints. The SJM overcomes this limitation. The contacts in the BPM model are oriented in the direction of the line connecting the centers of the particles involved in the contact. The SJM contacts are oriented perpendicular to the fracture plane irrespective of the relative position of the particles. Consequently, the particles can slide relative to each other in the plane of the fracture as if it were perfectly smooth. However, dilatant joint behavior can still be specified (as dilation angle) and enforced on the macroscopic level, irrespective of the details of the contact geometry on the microscopic level.

The SRM and its components are shown in Fig. 11. The BPM represents the intact rock; its deformation and damage. The pre-existing joints are represented explicitly, using the SJM. They can be treated deterministically, by specifying each discontinuity by its position and orientation as mapped in the field. However, for practical reasons, it is typically not possible to treat the DFN deterministically. Instead, fracturing in the rock mass is characterized statistically. Synthetic DFNs that are statistically equivalent (i.e., fracture spacing, orientation and size) to fracturing of the rock mass are generated and imported into the SRM using SJM (Fig. 11). A reasonable compromise often is to represent a few dominant structures (faults) with their deterministic position and orientation, and the rest of the fracturing in the rock mass (smaller structures), using a synthetic DFN.

One of the advantages of the SRM is that its components, the intact rock and the joints, can be mechanically characterized by

Table 1
Summary comparison between the *3DEC* and PKN solutions.

	PKN	*3DEC*	Error (%)
$w(0)$ (mm)	1.04×10^{-3}	1.07×10^{-3}	2.9
$p(0)$ (Pa)	2.71×10^{5}	2.99×10^{5}	9.3

[1] For interpretation of color in Figs. 10 and 19, the reader is referred to the web version of this article.

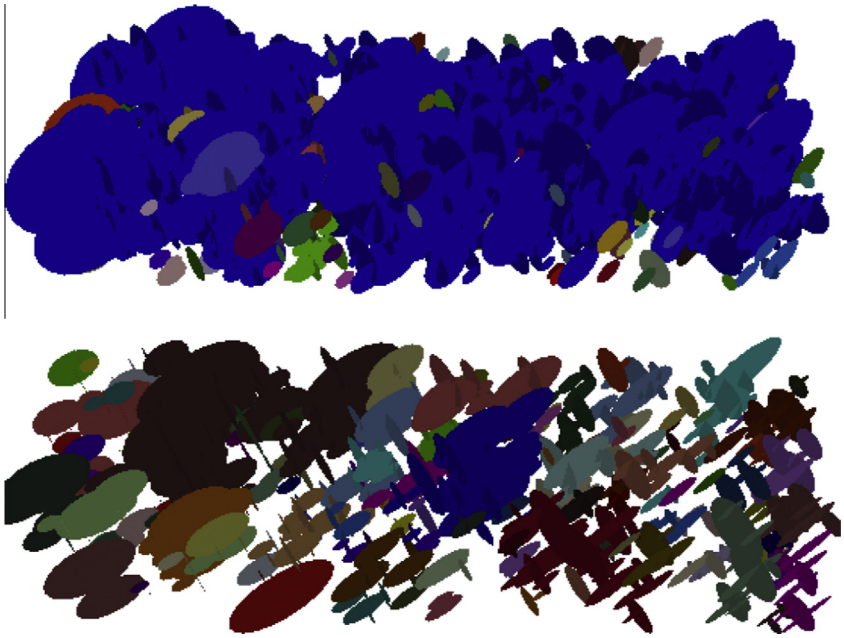

Fig. 7. Fully connected (top) and sparsely connected (bottom) *3DEC* DFN realizations. Clusters of connected fractures have same color [9].

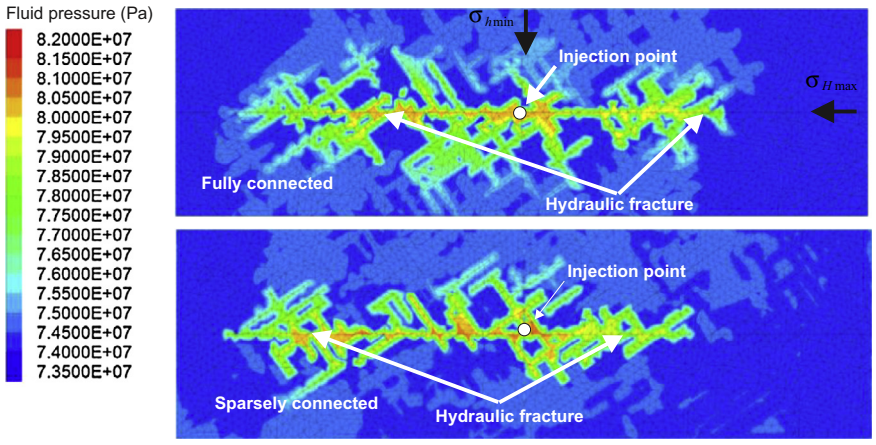

Fig. 8. Fluid pressure distribution on a horizontal cross-section cutting through the injection point after 50 min of injection for two DFN realizations [9].

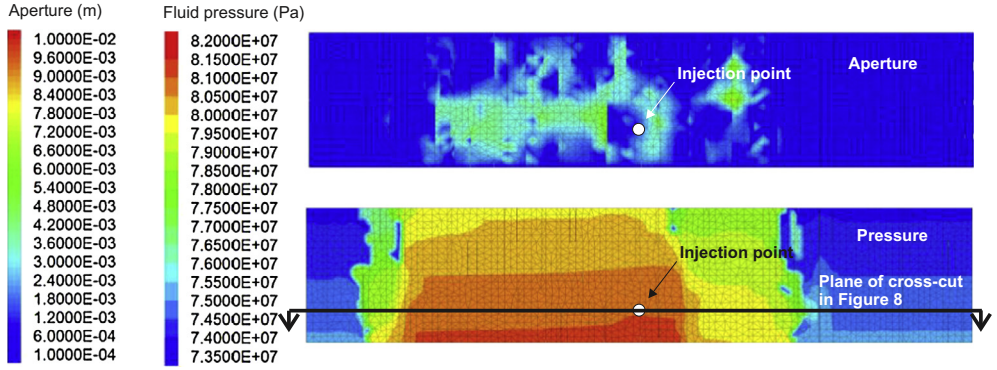

Fig. 9. Distribution of fracture aperture and fluid pressure for the sparsely connected DFN in the plane of hydraulic fracture [9].

standard laboratory tests. In current engineering practice, the rock mass properties on scales of interest (e.g., tunnel diameter, slope height or fracture length) are estimated by degrading, using empirical formulae, the properties determined on laboratory-scale samples. In contrast, the size effect is an outcome of SRM simulations: a function of the model size, DFN characteristics, and mechanical properties of the components (i.e., intact rock and joints). Thus, it is not necessary to rely on empirical relations to

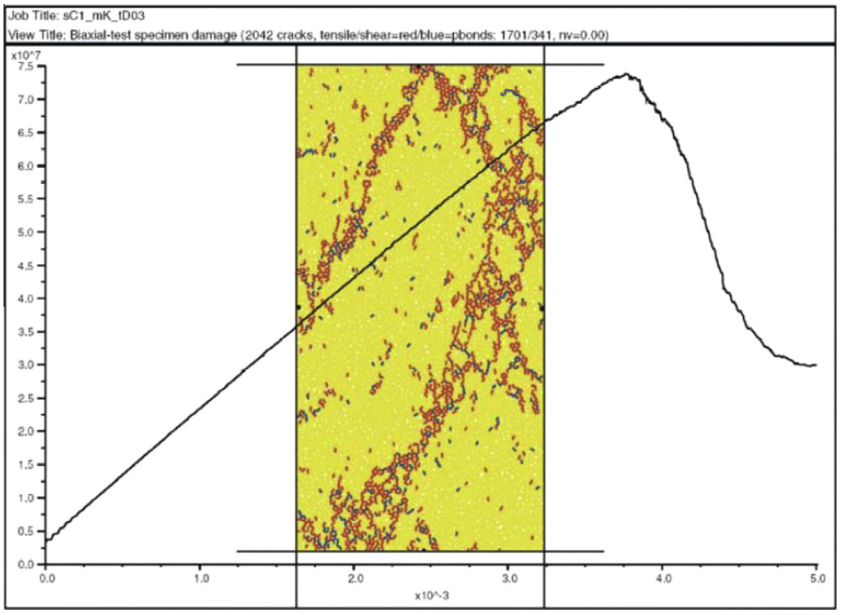

Fig. 10. Example of unconfined compressive test using bonded particle model (BPM).

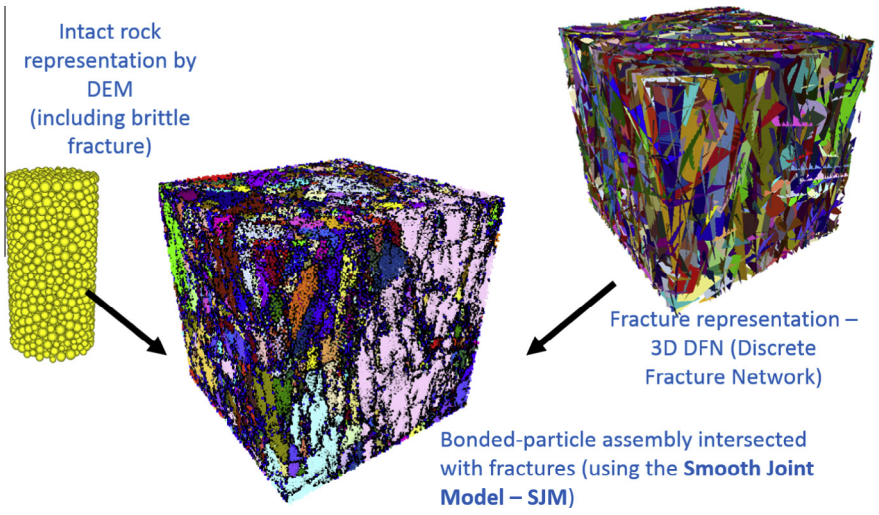

Fig. 11. Synthetic rock mass (SRM).

estimate the rock mass properties and to account for the size effect considering the size of the samples tested in the laboratory and the scale of interest in the model.

A new code, *HF Simulator*, was mentioned earlier in this paper. It is based on implementation of the SRM using a lattice, which is a simplified and computationally more efficient version of *PFC*. Despite simplifications, the lattice approach represents all of the physics that are important for the simulation of hydraulic fracturing.

4.2. Lattice

The lattice is a quasi-random 3D array of nodes (with given masses) connected by springs. It is formulated in small strain. The lattice nodes are connected by two springs; one representing the normal contact stiffness and the other representing the shear contact stiffness. The springs approximate the elasticity of the rock mass.

The lattice is created by multiplication of the periodic brick (p-brick) in three orthogonal directions. The p-brick is a quasi-random arrangement of nodes (which correspond to centers of packed spheres with slightly varying radii relative to half of the lattice resolution) within a cube of unit edge length. The p-brick is created thusly to allow perfect match of the bricks stacked by each other in all three orthogonal directions. The final model geometry is achieved by trimming of the "excess" lattice extending outside the analyzed domain. This approach allows for very fast model discretization. Changes in model resolution are achieved by simply rescaling the p-brick size. The mass of a node is equal to the p-brick mass divided by the number of the nodes within the p-brick. This approximation is acceptable because the distribution of the nodes within the p-brick is statistically uniform, and in this case, the lattice is used for solution of quasi-static problems.

The lattice spring properties are neither engineering nor microscopic material properties. Thus, in order to match engineering, macroscopic rock mass material properties such as Young's modulus, Poisson's ratio or tensile strength, the lattice spring properties need to be calibrated. The calibration is conducted in a similar way as for a *PFC3D* particle assembly, as discussed by Potyondy and Cundall [11] and Potyondy [20]. A simple dimensional and scaling

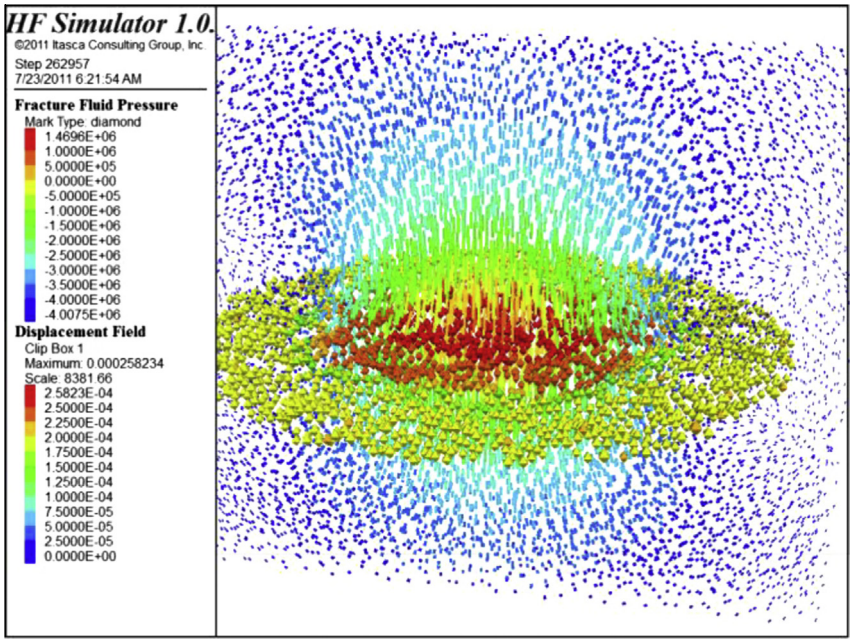

Fig. 12. View of pressure (Pa) field (icons colored according to magnitude) and cross-section of displacement (m) field (vectors colored according to magnitude).

analysis yields that the normal spring stiffness, k^N can be expressed as:

$$k^N = \alpha_k K_R R \tag{3}$$

where K_R is the material (rock) bulk modulus, R is the resolution, and α_k is the stiffness calibration factor, which varies as a function of arrangement of the nodes (or packing of the particles in *PFC3D*). However, because the lattice in *HF Simulator* is created using the p-brick and always the same arrangement of the nodes and their connectivity by the springs, the same calibration factor can be used irrespective of the resolution R. This factor is determined through test simulations and is built in the code. The effective Poisson's ratio of the lattice is a function of the ratio k^S/k^N. For example, if $k^S/k^N = 1$, the Poisson's ratio of the lattice is equal to zero. Similarly, the spring normal strength (in tension), $F^{N\max}$, can be expressed as:

$$F^{N\max} = \alpha_t T R^2 \tag{4}$$

where T is the rock mass macroscopic tensile strength, and α_t is the strength calibration factor, determined similarly as the stiffness calibration factor. The calibrated value of α_t is independent of the model resolution and is built in the code.

A simulation is carried out by solving an equation of motions (three translations and three rotations) for all nodes in the model using an explicit numerical method. The following is the central difference equation for the translational degrees of freedom:

$$\begin{aligned} \dot{u}_i^{(t+\Delta t/2)} &= \dot{u}_i^{(t-\Delta t/2)} + \Sigma F_i^{(t)} \Delta t/m \\ u_i^{(t+\Delta t)} &= u_i^{(t)} + \dot{u}_i^{(t+\Delta t/2)} \Delta t \end{aligned} \tag{5}$$

where $\dot{u}_i^{(t)}$ and $u_i^{(t)}$ are the velocity and position (respectively) of component $i (i = 1,3)$ at time $t, \Sigma F_i$ is the sum of all force-components i, acting on the node of mass m, with time step Δt. (The equations of motion for rotational degrees of freedom are analogous to those in Eq. (5).) The relative displacements of the nodes are used to calculate the force changes in the springs:

$$\begin{aligned} F^N &\leftarrow F^N + \dot{u}^N k^N \Delta t \\ F_i^S &\leftarrow F_i^S + \dot{u}_i^S k^S \Delta t \end{aligned} \tag{6}$$

where N denotes "normal," S denotes "shear," k is the spring stiffness, and F is the spring force. If the force exceeds the calibrated spring strength (either in tension or shear), the spring breaks and the microcrack is formed. For example, if $F^N > F^{N\max}$, then $F^N = 0, F_i^S = 0$and a "fracture flag" is set.

4.3. Fluid flow

A fluid-flow model and hydro-mechanical coupling are essential parts of *HF Simulator*. Fluid flow occurs through a network of pipes that connect fluid elements. These pipes are located at the centers of either broken springs or springs that represent pre-existing joints (i.e., springs intersected by the surfaces of pre-existing joints). (The code also can simulate porous medium flow through unfractured blocks as a way to represent leakoff. This capability is not discussed further in this paper.) The flow pipe network is updated automatically by connecting newly formed microcracks to the existing flow network. The model uses the lubrication equation [4] to approximate the flow within a fracture as a function of aperture. The flow rate along a pipe, from fluid node "A" to node "B," is calculated based on the following relation:

$$q = \beta k_r \frac{a^3}{12\mu} \left[p^A - p^B + \rho_w g \left(z^A - z^B \right) \right] \tag{7}$$

where a is hydraulic aperture, μ is viscosity of the fluid, p^A and p^B are fluid pressures at nodes "A" and "B", respectively, z^A and z^B are elevations of nodes "A" and "B," respectively, ρ_w is fluid density, and g is the acceleration due to gravity. The relative permeability, k_r is a function of saturation, s, with respect to wetting fluid:

$$k_r = s^2(3 - 2s) \tag{8}$$

This function is selected because it represents an s-shaped curve with zero relative permeability for unsaturated conditions and relative permeability equal to one at full saturation.

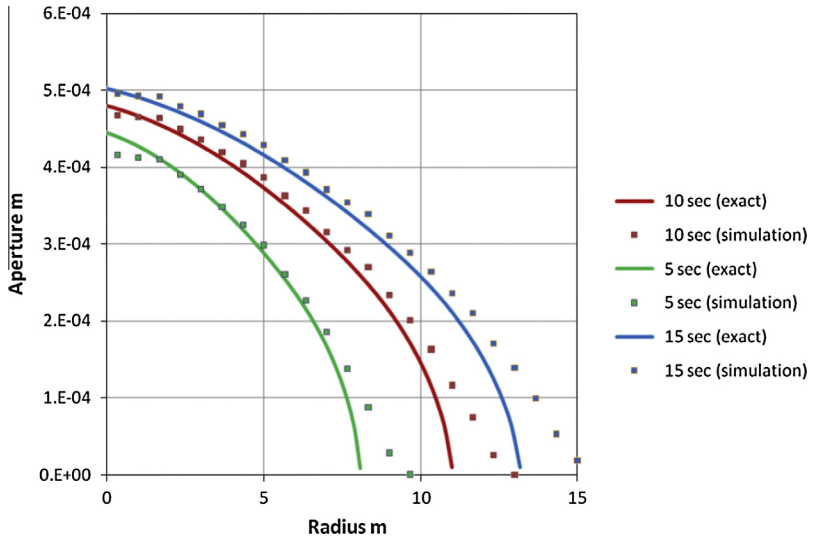

Fig. 13. Aperture profiles for three times.

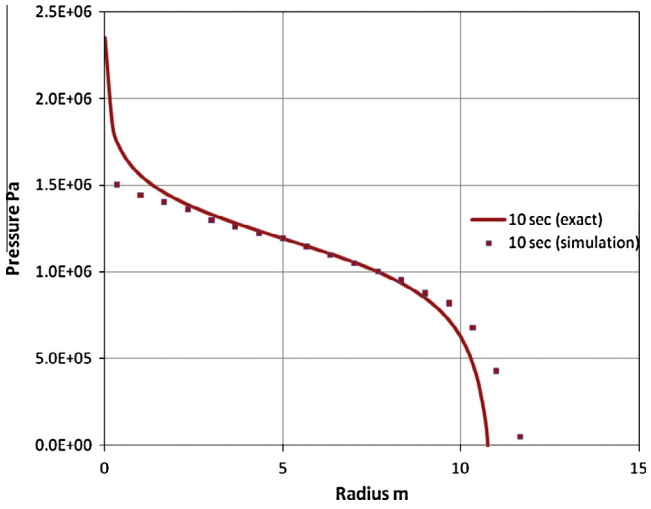

Fig. 14. Pressure profile at 10 s.

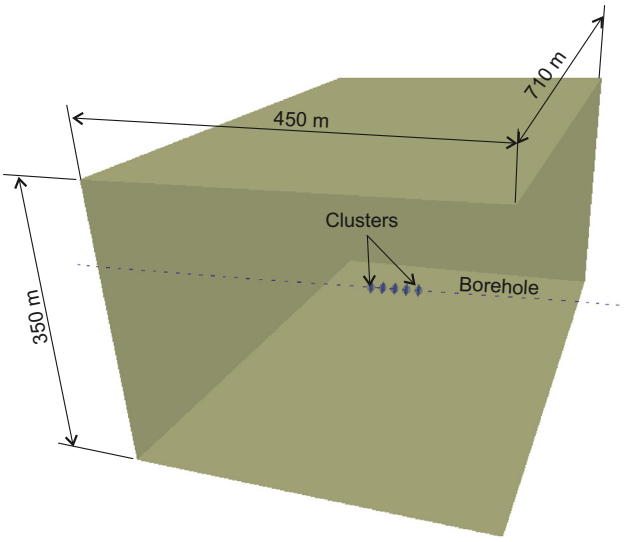

Fig. 15. Geometry of the model for a stage with multiple clusters.

β is a dimensionless calibration parameter, and is a function of resolution. β is used to match conductivity of a pipe network to the conductivity of a joint represented by parallel plates with aperture a. The calibrated relation between β and the resolution is built into the code.

4.4. Hydro-mechanical coupling

In *HF Simulator*, the mechanical and flow models are fully coupled.

1. Fracture permeability depends on the initial aperture and on the subsequent deformation of the solid model.
2. Fluid pressure affects both deformation and the strength of the solid model. Effective stress calculations are carried out.
3. The deformation of the solid model affects the fluid pressures. In particular, the code can predict changes in fluid pressure under undrained conditions.

A new coupling scheme [22] in which the relaxation parameter is proportional to $K_R a/R$ is implemented in *HF Simulator*. (K_R is rock bulk modulus and R is the lattice resolution.) This scheme allows larger explicit time steps and faster simulation times compared to conventional methods that use fluid bulk modulus as a relaxation parameter.

4.5. Verification test: penny-shaped crack propagation in medium with zero toughness

The response of rock to injection of fluid depends on fracture toughness, the viscosity of the fluid and the rate of leakoff. In the case of zero fracture toughness and no leakoff, the response is viscosity-dominated. This scenario corresponds to the "M-asymptote" identified by Peirce and Detournay [23]. This condition is used for model verification.

In the simulated example, fluid is injected at a constant rate into a penny-shaped crack with small initial aperture (10^{-5} m). The crack has zero normal strength, and the in-situ stresses are also zero. Thus, the test conditions approximate those of the analytical solution for the no-lag case (i.e., no fluid pressure tension cut-off)

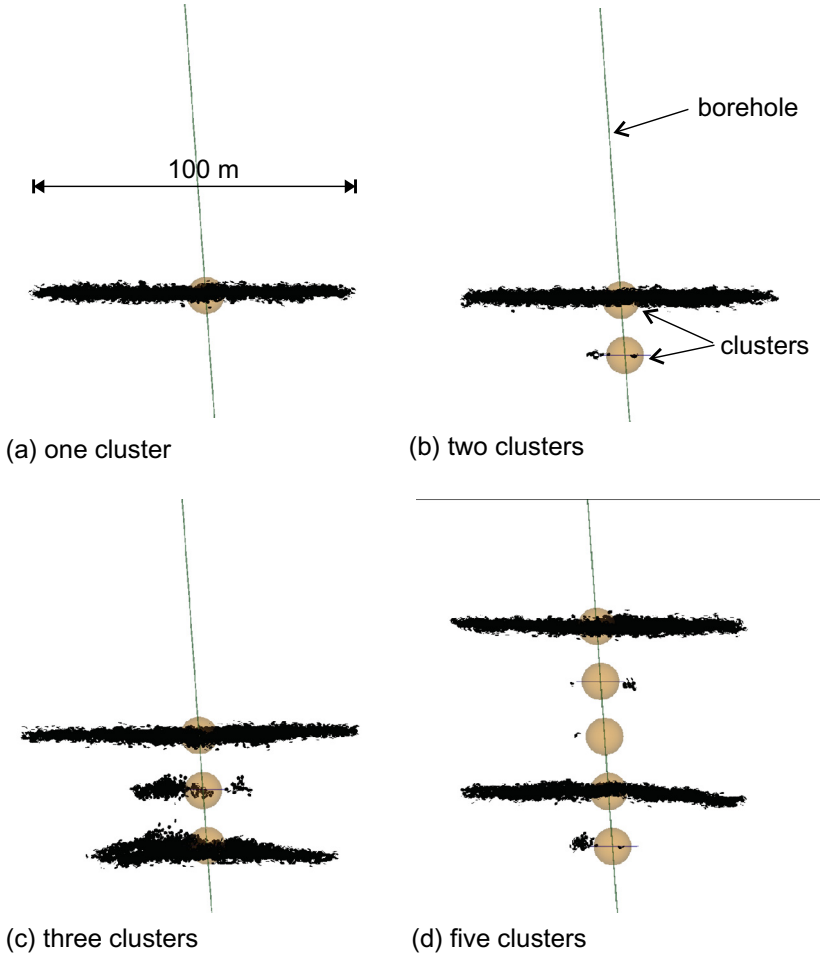

Fig. 16. Interaction of multiple clusters within one stage: plan view.

provided by Peirce and Detournay [23]. The injection rate is 0.01 m^3/s; the dynamic viscosity is 0.001 Pa s. The mechanical properties of the rock are characterized by Youngs modulus of 7×10^{10} Pa and Poissons ratio of 0.22. Fig. 12 provides a visualization of the state of the model at 10 s of elapsed time. Note that pressures are negative in the outer annulus of the flow disk.

Fig. 13 shows the aperture profiles at three times during the simulation — averaged numerical results (for 30 radial distances), together with asymptotic solutions (derived from the equations of Peirce and Detournay [23]). Fig. 14 shows the pressure profile at 10 s, together with the asymptotic solution. Note that there is some "mismatch" at small and large radial distances: at small distances, the numerical source is a finite volume, rather than a point source (which is assumed in the exact solution); at large distances, the finite initial aperture allows seepage ahead of the fracture tip (compared to zero seepage in the exact solution, which assumes zero initial aperture).

4.6. Example application

Example problems demonstrating the application of *HF Simulator* to simulation of hydraulic fracturing under typical field conditions are presented in this section. Fracture propagation in homogeneous (unfractured) and fractured media is analyzed. These problems involve a single treatment stage along a horizontal wellbore segment with a different number of clusters (between one and five, resulting in different stage lengths) at a spacing of 17.5 m (Fig. 15). The model domain is 710 m × 450 m × 350 m, and a lattice resolution of 6 m was selected. The objective of this model was to simulate fracture propagation at length scales corresponding to a hydraulic fracture radius in the order of 100 m. At such length scales, the wellbore radius and stress concentrations around the wellbore are inconsequential and could be neglected. (Thus, there was no need to represent the wellbore and to reduce the resolution, which then would adversely affect the model size and the simulation time.) The fluid is injected through clusters, defined as spherical domains properly scaled relative to the model resolution (i.e., the cluster radius is typically greater than few lattice resolutions).

Fluid is injected into the stage at rate of 0.0265 m^3/s (10 barrels per minute or bpm) for 1300 s. The rate was then increased to 0.053 m^3/s (20 bpm). The model solves wellbore hydraulics and interaction between the wellbore and the clusters. Thus, the specified injection rate is distributed between the clusters as a function of resistance to flow and fracture propagation from each cluster. The injection rate typically is not evenly distributed between the clusters. The depth of the horizontal segment of the wellbore is 780 m. The vertical stress was specified as 20.7 MPa. The horizontal stress state is anisotropic, with $S_{H\max} = 15.5$ MPa and $S_{h\min} = 10$ MPa. The least principal stress is aligned with the horizontal section of the wellbore. This stress state favors crack propagation in the direction normal to the horizontal section of the wellbore. In order to initiate the fluid calculation, fluid-filled joints

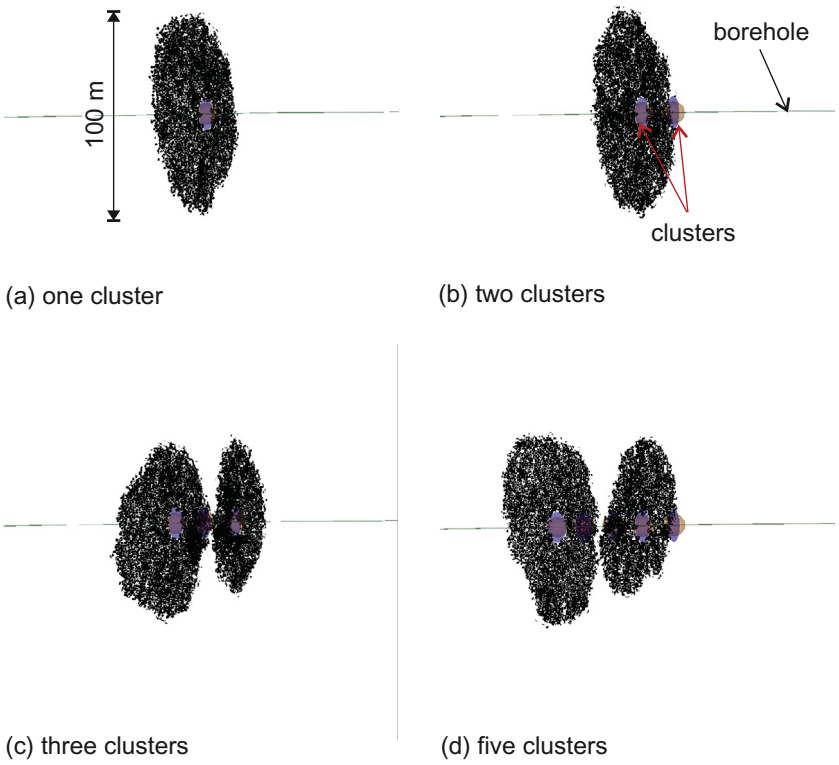

Fig. 17. Interaction of multiple clusters within one stage: oblique side view.

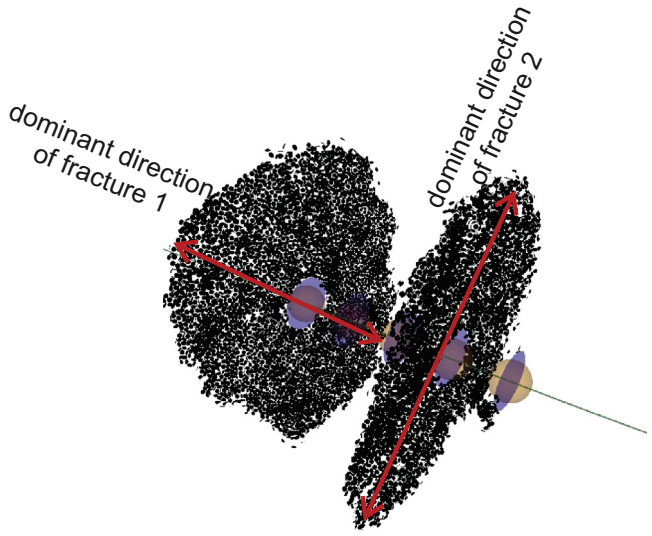

Fig. 18. Anisotropic fracture growth.

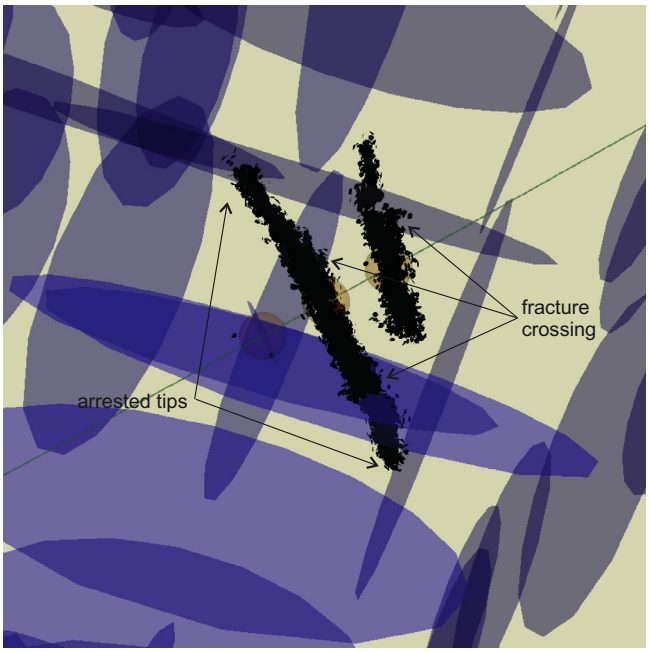

Fig. 19. Interaction between hydraulic fractures and pre-existing joints.

have been placed at the center of each cluster; these joints are slightly larger than the cluster size. The fracture initiation can be simulated in the model, but, as mentioned in the previous paragraph, the resolution necessary for accurate simulation of fracture initiation would make the model inefficient for simulation of fracture propagation during fluid injections lasting on the order of hours. The initial apertures in these joints was set to 0.1 mm.

The simulation results after 2400 s of injection are shown in Figs. 16 and 17, in plan and side views, respectively. The black disks (or dots) in the plots indicate locations of microcracks. The microcracks apparently coalesce to form the macroscopic hydraulic fractures. The stage with a single cluster propagates an approximately

penny-shaped hydraulic fracture with radius of 50 m. The stage with two clusters propagates only one fracture of approximately the same radius. The cluster that first started propagating a fracture, due to random variation of the conditions within the lattice and/or slightly higher pressure due to resistance to flow along the wellbore, created a "stress shadow," and prevented the propagation of the hydraulic fracture from the second cluster. The cases with three and five clusters both propagated two hydraulic fractures from non-adjacent clusters. This result seems to be consistent with the hypothesis based on field observations that stages with multiple clusters may not develop hydraulic fractures from all clusters; there may or may not be more than one hydraulic fracture. Another interesting result of the numerical model is that multiple fractures within one stage are not penny-shaped, but more elliptical as illustrated in Fig. 18. The directions of the major axes of the ellipses in the plane of the hydraulic fracture, are offset by an angle, which is another indication of interaction between the fractures and the "stress shadow" effect [24].

The case with three clusters within the stage also was simulated in the model with the fracture network that was explicitly represented. The DFN consists of two subvertical fracture sets, striking at 45° relative to the directions of the horizontal principal stresses. The model results are shown in Fig. 19. The blue[1] disks represent pre-existing joints. The model illustrates different modes of interaction between hydraulic fractures and pre-existing joints. The model exhibits both crossing interaction but also arrest of hydraulic fracture and diversion of flow into the pre-existing joint. The mode of interaction is a function of incidence angle and stress conditions in the planes of pre-existing joints.

5. Conclusions

The DFN can have a profound effect on hydraulic fracture propagation, hydraulic fracture interaction with the surrounding rock mass, and ultimately the fracture effectiveness of the stimulation. As the examples indicate, analysis of rock mass stimulation by fluid injection requires analytical tools, such as numerical models based on DEM or SRM, which can represent discontinuities explicitly. The FNE approach, based on the use of these numerical models and field observations, promises to be an engineering design tool for operations that involve complex coupled processes in complex geological environments in which explicit representation of pre-existing fractures is essential.

HF Simulator is a powerful three-dimensional simulator for representing hydraulic fracturing in jointed rock mass. The code allows the main mechanisms (nonlinear mechanical response, fluid flow in joints and hydro-mechanical coupling) to be reproduced. The formulation of *HF Simulator* is based on a quasi-random lattice of nodes and springs. The springs between the nodes break when their strength (in tension) is exceeded. Breaking of the springs corresponds to the formation of microcracks, and microcracks may link to form macrofractures. The SJM (smooth joint model) is used to represent pre-existing joints in the model. It allows simulation of sliding of a pre-existing joint in the model, unaffected by the apparent surface roughness resulting from lattice resolution and random arrangement of lattice nodes.

The model is fully coupled hydro-mechanically. There are several ways in which fluid interacts with the rock matrix. First, fluid pressures may induce opening or sliding of the fractures. Second, mechanical deformation of fractures causes changes in fluid pressure. Third, the mechanical deformation changes the permeability of the rock mass as the joint apertures change. The new code is a promising tool for simulation and understanding of complex processes, including propagation of hydraulic fracture and its interaction with a DFN, during stimulation.

Acknowledgements

The development of the numerical code, *HF Simulator*, described in this paper was funded by BP America. The authors would like to thank BP America for their support. Christine Detournay, Jim Hazzard, Matt Purvance, Azadeh Riahi, Maurilio Torres, and Varun of Itasca Consulting Group, Inc. are thanked for their valuable work on *HF Simulator* and application of DEM models to hydraulic fracturing problems.

References

[1] Cipolla CL, Lolon EP, Erdie JC, Tathed V. Modeling well performance in shale-gas reservoirs. Presented at the SPE/EAGE reservoir characterization and simulation conference held in Abu Dhabi, UAE, October 19–21; 2009.
[2] Cundall PA. A computer model for simulating progressive large-scale movement in blocky rock systems. In: Proceedings of the symposium of the international society of rock mechanics (Nancy, France, 1971) vol. 1, Paper No. II-8; 1971.
[3] Pine RJ, Cundall PA. Applications of the fluid-rock interaction program (FRIP) to the modelling of hot dry rock geothermal energy systems. In: Proceedings of the International Symposium on Fundamentals of Rock Joints, Bjorkliden; 1985. p. 293–302.
[4] Batchlor GK. An introduction to fluid dynamics. Cambridge at the University Press; 1967.
[5] Itasca Consulting Group, Inc. 3DEC (Three-Dimensional Distinct Element Code), Version 5.0. Minneapolis, Minnesota, USA; 2007.
[6] Cundall PA. Formulation of a three-dimensional distinct element model – Part I: A scheme to detect and represent contacts in a system of many polyhedral blocks. Int J Rock Mech Min Sci 1988;25:107–16.
[7] Hart R, Cundall PA, Lemos J. Formulation of a three-dimensional distinct element model – Part II: Machanical calculations for motion and interaction of a system of many polyhedral blocks. Int J Rock Mech Min Sci 1988;25:117–26.
[8] Damjanac B. A three-dimensional numerical model of water flow in a fractured rock mass. PhD thesis, University of Minnesota, Minneapolis; 1996.
[9] Savitski AA, Lin M, Riahi A, Damjanac B, Nagel NB. Explicit modeling of hydraulic fracture propagation in fractured shales. IPTC-17073-MS; 2013.
[10] Zhang F, Maxwell SC, Damjanac B. Modeling of fault activation induced by hydraulic fracturing – a Horn River basin case study. Hyd Fract J 2015;2(1):26–33.
[11] Potyondy DO, Cundall PA. A bonded-particle model of rock. Int J Rock Mech Min Sci 2004;41:1329–64.
[12] Pierce M, Mas Ivars D, Cundall PA, Potyondy DO. A synthetic rock mass model for jointed rock. In: Eberhardt E et al., editors. Rock mechanics: meeting society's challenges and demands (1st Canada-U.S. rock mechanics symposium, Vancouver, May 2007). Fundamentals, new technologies & new ideas, vol. 1. London: Taylor & Francis Group; 2007. p. 341–9.
[13] Itasca Consulting Group, Inc. PFC2D (Particle Flow Code in 2 Dimensions), Version 5.0. Minneapolis: Itasca; 2008.
[14] Itasca Consulting Group, Inc. PFC3D (Particle Flow Code in 3 Dimensions), Version 5.0. Minneapolis: Itasca; 2008.
[15] Maxwell SC, Cipolla C. What does microseismicity tell us about hydraulic fracturing? SPE 146932, SPE annual technical conference and exhibition, 30 October–2 November 2011. Colorado, USA: Denver; 2011.
[16] Pettitt W, Pierce M, Damjanac B, Hazzard J, Fairhurst C, Gil I, et al. Fracture network engineering for hydraulic fracturing. Lead Edge 2011;30(8):844–53. http://dx.doi.org/10.1190/1.3626490.
[17] Hazzard JF, Young RP, Maxwell SC. Micromechanical modeling of cracking and failure in brittle rocks. J Geophys Res 2000;105(B7):683–97.
[18] Perkins T, Kern L. Widths of hydraulic fractures. J Pet Tech 1961;222:937–49.
[19] Jaeger JC, Cook NGW. Fundamentals of rock mechanics. 3rd ed. Chapman and Hall; 1979.
[20] Potyondy DO. The bonded-particle model as a tool for rock mechanics research and application: current trends and future directions. Geosyst Eng 2014;17(6):342–69. http://dx.doi.org/10.1080/12269328.2014.998346.
[21] Valkó P, Economides MJ. Hydraulic fracture mechanics. John Wiley and Sons; 1995.
[22] Cundall PA. Lattice method for brittle, jointed rock. In: Continuum and distinct element numerical modeling in geomechanics. Itasca International, Inc.; 2011. ISBN: 978-0-9767577-2-6.
[23] Peirce A, Detournay E. An implicit set method for modeling hydraulically driven fractures. Comput Methods Appl Mech Eng 2008;197:2858–85.
[24] Nagel N, Zhang F, Sanchez-Nagel M, Lee B, Agharazi A. Stress shadow evaluations for completion design in unconventional plays. Society of petroleum engineers; 2013. doi:http://dx.doi.org/10.2118/167128-MS.